Construction by Molecular Dynamics Modeling and Simulations of the Porous Structures Formed by Dextran Polymer Chains Attached on the Surface of the Pores of a Base Matrix: Characterization of Porous Structures

X. Zhang,[†] J.-C. Wang,[†] K. M. Lacki,[‡] and A. I. Liapis*[,†]

Department of Chemical and Biological Engineering and Biochemical Processing Institute, University of Missouri-Rolla, Rolla, Missouri 65409-1230, and GE Healthcare, Protein Separations, Amersham Biosciences AB, Björkgatan 30, SE-751 84 Uppsala, Sweden

Received: June 23, 2005; In Final Form: September 9, 2005

Significant increases in the separation of bioactive molecules by using ion-exchange chromatography are realized by utilizing porous adsorbent particles in which the affinity group/ligand is linked to the base matrix of the porous particle via a polymeric extender. To study and understand the behavior of such systems, the M3B model is modified and used in molecular dynamics (MD) simulation studies to construct porous dextran layers on the surface of a base matrix, where the dextran polymer chains and the surface are covered by water. Two different porous polymer layers having 25 and 40 monomers per main polymer chain of dextran, respectively, are constructed, and their three-dimensional (3D) porous structures are characterized with respect to porosity, pore size distribution, and number of conducting pathways along the direction of net transport. It is found that the more desirable practical implications with respect to structural properties exhibited by the porous polymer layer having 40 monomers per main polymer chain, are mainly due to the higher flexibility of the polymer chains of this system, especially in the upper region of the porous structure. The characterization and analysis of the porous structures have suggested a useful definition for the physical meaning and implications of the pore connectivity of a real porous medium that is significantly different than the artificial physical meaning associated with the pore connectivity parameter employed in pore network models and whose physical limitations are discussed; furthermore, the methodology developed for the characterization of the three-dimensional structures of real porous media could be used to analyze the experimental data obtained from high-resolution noninvasive three-dimensional methods like high-resolution optical microscopy. The MD modeling and simulations methodology presented here could be used, considering that the type and size of affinity group/ligand as well as the size of the biomolecule to be adsorbed onto the affinity group/ligand are known, to construct different porous dextran layers by varying the length of the polymeric chain of dextran, the number of attachment points to the base matrix, the degree of side branching, and the number of main polymeric chains immobilized per unit surface area of base matrix. After the characterization of the porous structures of the different porous dextran layers is performed, then only a few promising structures would be selected for studying the immobilization of adsorption sites on the pore surfaces and the subsequent adsorption of the bioactive molecules onto the immobilized affinity groups/ligands.

1. Introduction

In the past twenty years, advances in molecular biology and separation science have resulted in large-scale production of diagnostics and biotherapeutics. In downstream purification of bioactive macromolecules, the capture step serves the dual purpose of removing the bulk of impurities and concentrating the product of interest, and because of this, ion-exchange chromatography (IEC) has become a very important separation method in downstream purification for the isolation of peptides, enzymes, and proteins.[1−18]

It is very important in the IEC systems to use adsorbent particles that can provide the highest possible breakthrough capacity for the desired bioactive molecules. It is found that a high breakthrough capacity can be realized[7] by utilizing porous adsorbent particles in which the affinity group/ligand is linked to the base matrix of the porous particles via an extender, as shown schematically in Figure 1. The preferred attachment of the positively or negatively charged affinity group/ligand to the base matrix via an extender is covalent, and the extender may be in the form of a polymer.[7,19] Suitable extenders have been found[7,19] to be polysaccharides such as dextran, while cross-linked agarose providing desired porosity and stability has been found to be a suitable base matrix.[7,19] Typical affinity groups/ligands are (a) positively charged groups (e.g., primary, secondary, tertiary, or quaternary amine groups[7,8]) and (b) negatively charged groups (e.g., carboxyl, phosphoric acid, sulfonic acid[7,9]). The positive effect caused by the extender is speculatively considered[7] to reside in the fact that it will provide the inner surfaces (pore surfaces) and/or outer surfaces of the base matrix with a flexible polymer layer that is permeable to bioactive molecules; this is thought to cause an increase in the effective volume as well as in the steric availability of the affinity groups/ligands for the charged biomolecules to be adsorbed and, this

* To whom all correspondence should be addressed. E-mail: ail@umr.edu. Telephone: (573) 341-4414. Fax: (314) 965-9329.
[†] Department of Chemical and Biological Engineering and Biochemical Processing Institute.
[‡] GE Healthcare, Protein Separations.

10.1021/jp053421h CCC: $30.25
Published on Web 10/15/2005

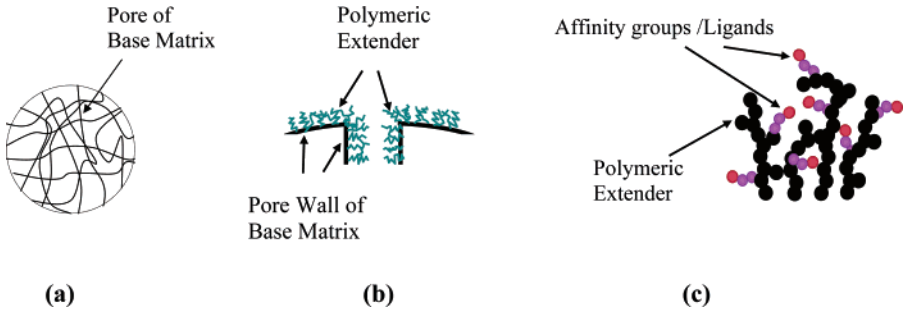

Figure 1. Schematic representation of a porous adsorbent particle employed in ion-exchange chromatography systems for the separation of biomolecules. (a) Porous base matrix. (b) Polymeric extenders attached on the pore wall of base matrix. (c) Affinity groups/ligands attached on polymeric extenders.

could, in turn, increase the mass transfer rate[10,11,15−18] as well as the available total capacity for adsorption.

To control the flexibility of the extender, the base matrix is first activated by using the proper density of reactive groups per unit surface area, and then the extender is linked to the matrix by reaction with the reactive groups that had been introduced on the surface of the pores of the base matrix; this process represents Stage I in the construction of adsorbent particles that employ polymeric extenders. Stage I produces a porous polymeric structure that is covalently attached on the surface of the pores of the base matrix, and is followed by Stage II, where the positively or negatively charged affinity groups/ligands are attached[7] on the polymeric extenders to construct the adsorbent particles that are employed in IEC systems. The performance of the adsorbent particles for the effective separation of a desired charged biomolecule will depend on the structure of the porous layer formed by the polymeric extenders on which the charged affinity groups/ligands are attached during Stage II, the chemistry of the attached ligands, and, of course, on the density distribution of the charged affinity groups in this porous polymer layer that is covalently attached on the surface of the pores of the base matrix. However, the properties of the adsorbent particles that one obtains at the end of Stage II will depend, of course, on the properties of the structure of the porous polymer layer that one obtained at the end of Stage I because the initial condition of Stage II is represented by the final condition of Stage I.

In this work, molecular dynamics (MD) modeling and simulations are used to construct a porous polymer layer from dextran polymer chains that are covalently attached on the surface of a base matrix immersed in an aqueous solution. Thus, the goal of this work is to model and simulate the structure of the porous polymer layer being constructed in Stage I, as well as to characterize the properties of the porous polymer layer obtained at the end of Stage I; it is worth mentioning here that the results of this work are found to be useful in providing a physical mechanistic reasoning for the interpretation and meaning of experimental observations about the behavior of porous polymer layers formed from dextran polymer chains. Future work will characterize the porous polymer layer obtained at the end of Stage II, where the affinity groups/ligands would have been attached on the polymer chains and would have, thus, established an adsorbent porous layer on whose active sites (affinity groups/ligands) a desired charged biomolecule could be physically adsorbed. The adsorption process of the charged biomolecule could be considered to represent Stage III of a study whose scope would be to employ MD modeling and simulations to guide the design, construction, and evaluation of the performance of adsorbents that can efficiently[1−19] adsorb the desired charged biomolecule.

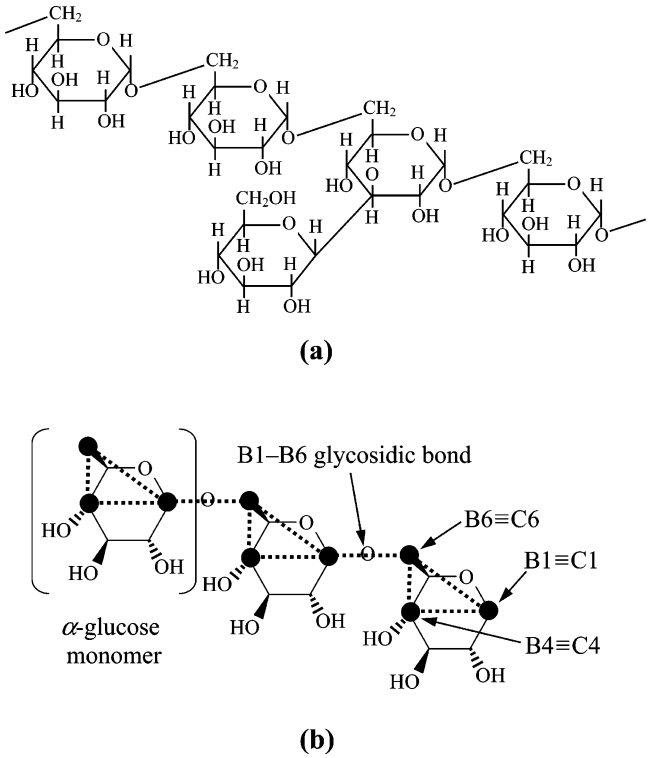

Figure 2. (a) Atomistic structure of a fragment of dextran molecule. (b) Structure of a fragment of dextran molecule using the modified coarse-grain M3B model; beads B1, B4, and B6 of the M3B model correspond to the positions of the carbons C1, C4, and C6, respectively in the atomistic model.

2. System Formulation and Simulation Models and Methods

Dextran is an α-D-(1 → 6)-linked glucan with side chains that are mostly 1−2 glucose units long[7,19] and are attached to the O-3 of the backbone units;[19] the structure of a fragment of a dextran polymer chain is shown in Figure 2a. Estimates of the density of the dextran polymer chains attached on the pore surface of different adsorbent particles suggest that the value of the density could vary from one polymer chain per 9500 Å^2 to one polymer chain per 850 Å^2, and the degree of side branching is approximately 5%, with mostly 1−2 glucose units long. To ensure timely, efficient MD simulations as well as reasonable statistics for this work, 10 dextran chains with 5% side branching and 1−2 glucose units as side chains on a 100 Å × 100 Å surface are employed in this work for the construction of model porous layers formed by the dextran polymer extenders. In separation operations employed in practice, the adsorbent particles are completely immersed in an aqueous solution, and thus, the water molecules are occupying

the pores of the dextran layer and also form a bulk phase in contact with the dextran layer; from this bulk phase, biomolecules are transported toward the vacant adsorption sites and are adsorbed. Therefore, it is necessary and important for our simulation model system to include a thick layer of water on top of the dextran chains that exhibits proper water density and represents the solution bulk phase; the thickness of the layer of water was taken to be 30 Å above the 100 Å length along the *z* direction that was corresponding to the location of the bead being in the farthest from the base matrix position along the *z* direction. To satisfy this necessary requirement, it was determined that approximately 30000 water molecules were needed and had to be considered in our simulation system. Thus, the resultant model system is computationally very demanding for MD simulations. For such circumstances, it has become an increasingly common practice to coarse-grain the model system. The essence of coarse-grain models is to sacrifice finer details in order to make significantly larger time and length scales accessible to simulation studies. Numerous coarse-grain models have been shown to reproduce accurately relevant structural and dynamical features for various systems studied and reported in the literature.[20−25]

Molinero and Goddard[20] have recently developed a rigorous coarse-grain model for carbohydrates that is called the M3B model. As shown in Figure 2b, this model represents one glucose monomer with three beads located at C1, C4, and C6, and furthermore, it includes bond-bending and torsion motions. It has been parametrized to produce realistic size, conformations, glass transition temperature, and energetic interactions of α-D-(1 → 4)-linked glucans and their water mixtures that are in good agreement with experimental observations. The M3B model has, in general, better resolution in providing structural and dynamical properties than many widely used bead-spring models,[24,25] where one bead usually represents several monomers and the bead-spring models tend to capture generic characteristics of polymeric systems. Furthermore, the M3B model has a rigorous one-to-one correspondence with and can be mapped into the full atomistic representation of the glucans. In this work, the M3B model is adopted with a modification in order to become applicable to dextran, because dextran has an α(1 → 6) linkage instead of an α(1 → 4) linkage. A schematic representation of the atomistic and coarse-grain models of dextran is shown in Figure 2b, and the modification of the M3B model is required because different bending and torsion angles around the C1−O−C6 bonds are needed to reflect the chemical structure of α(1 → 6)-linked glucose monomers. It is important to note here that, in the construction of the M3B model, the beads are considered to be electrically neutral, but their mutual interactions have been parametrized to include the effects of core repulsion and van der Waal and electrostatic interactions.

It has been shown[16,21] that water modeled as an implicit continuum medium may not provide an appropriate excluded volume effect and proper biomolecular conformations at the molecular level. However, the task of simulating 30000 water molecules by using an atomistic model for the water molecules, such as the TIP5P model[16,17] that was used in our previous studies,[16,17] requires a tremendous amount of computational time, and the possible improved accuracy of our simulation results with regard to the porous structure of the dextran layer may not be significant because the coarse-grain M3B model defines the level of the overall resolution. An alternative explicit model that has been quite commonly used in existing studies[20] and is employed in this work considers that each water molecule is coarse-grained into a sphere whose size reflects that of a genuine water molecule whose size is interestingly similar to the size of the beads of the M3B model; the size of each bead in the M3B model is approximately equal to 3 Å. As a result, the whole model system in this work can be rigorously converted to a full atomistic model system, when certain finer-scale properties become the aim of investigation in our future studies. To account for the charge-screening effect of water, its dielectric constant can be used in the calculation of Coulombic interaction. However, in this work, the use of the dielectric constant becomes unnecessary because the M3B beads are electrically neutral, as discussed above.

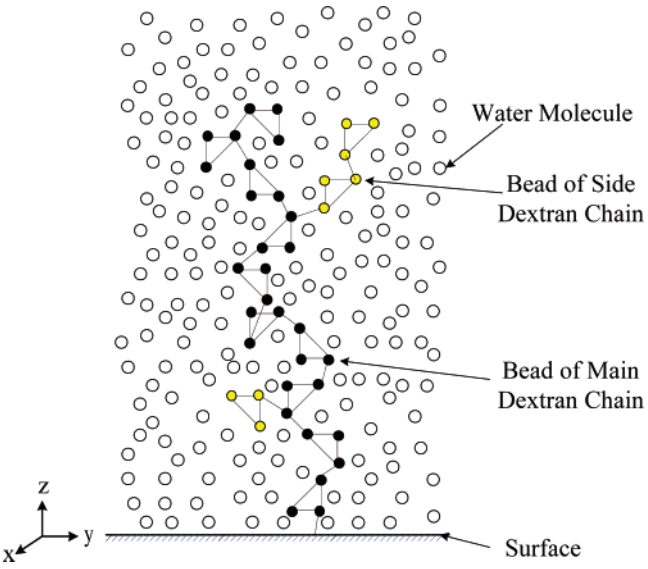

Figure 3. Schematic representation based on the beads of the modified M3B model of a dextran polymer chain attached on the surface of a base matrix, where the beads of the dextran polymer are surrounded by water molecules.

The region of the porous dextran layer that is located farthest from the surface of the base matrix would play a significantly more important role with respect to (a) the transport from the bulk liquid phase of the biomolecules and (b) the adsorption of the biomolecules onto the vacant adsorption sites than the region of the porous polymer layer located next to the surface of the base matrix. Because the base matrix is not included in our simulation system, we randomly fixed the first bead of each of the 10 dextran polymer chains on the *xy* plane at $z = 0$ and applied periodic boundary conditions along the lateral *x* and *y* directions. Without a periodic boundary condition along the *z* direction, the water layer develops a liquid−vacuum interface 30 Å above the uppermost surface of the dextran porous polymer layer, as was discussed earlier and which is considered to have negligible direct influence on the pore structure formed by the dextran polymer chains. A schematic representation of the attachment of a dextran polymer chain on the surface of the base matrix as well as the water molecules surrounding the beads of the polymer chain are shown in Figure 3. While this may not be completely realistic, the upper part (region) of the resultant dextran porous layer is expected to be only minimally affected. The experimental data[19] indicate that the performance of the adsorbent particles depends strongly on the chain length of the dextran polymers attached to the base matrix. Therefore, an important goal of this work is to examine the effect of the chain length of the polymer on the structure of the porous dextran layer, especially in the upper part of the dextran layer. For this purpose, two chain lengths are considered in this work, one with 25 monomers per main polymer chain and another with 40 monomers per main polymer chain, both with 5% side

branching and one end attached to and immobilized on the surface of the base matrix. One or two glucose monomers are randomly chosen for the formation of a single side chain. The locations of the side chains are chosen randomly on the main linear dextran chain and bonded to the C4 positions of the monomers (B4 beads) in the main chain.

In the model system, the interaction between the coarse-grain beads of the dextran polymer chains is expressed as a sum of valence and nonbonded terms[20]

$$E_t = E_V + E_{nb} \tag{1}$$

where E_t represents the total energy for dextran, E_V denotes the valence potential energy within the dextran polymer chains, and E_{nb} represents the nonbonded potential energy between the coarse-grain beads of the dextran polymer chains. The bonds between two consecutive coarse-grain beads in the dextran are constrained to their equilibrium length by applying the SHAKE algorithm.[26,27] As a result, the valence potential energy, E_V, is represented by three-body interactions associated with the bending angle between three consecutive beads, and four-body interactions associated with the torsion angle between four consecutive beads[20]

$$E_V = E_{bending} + E_{torsion} \tag{2}$$

The coarse-grain bending motions are considered to be harmonic,[20] and their potential energy is given by eq 3

$$E_{bending}(\theta) = \frac{1}{2}k_\theta(\theta - \theta_0)^2 \tag{3}$$

where θ represents the bending angle between connected coarse-grain particles, θ_0 denotes the coarse-grain angle equilibrium position, and k_θ is the coarse-grain bending force constant.

For the four-body valence interactions, each coarse-grain torsional angle energy is considered[20] to be represented by a sum of shifted dihedral functions

$$E_{torsion}(\varphi) = \sum_j \frac{1}{2}B_j(1 + \cos(j\varphi - \varphi_j^\circ)) \tag{4}$$

where the coarse-grain torsional angle $\varphi = \varphi_{inkl}$ denotes the angle between the planes formed[20] by *ink* and *nkl* (*n*, *k*, *l* are B1, B4, or B6), the sum is over the different *j* terms of the potential, each with a different integral periodicity *j*, barrier B_j, and phase φ_j°.

In the coarse-grain model employed in this work for the dextran polymer chains, the values of the equilibrium bond length for the different bond types, the values of the parameter k_θ (eq 3), as well as the values of the parameters B_1, B_2, and B_3 (eq 4), were obtained from the data presented in Tables 2, 3, and 4, respectively, in the work of Molinero and Goddard.[20] Because of the difference between the link of the glucose monomers in the dextran polymer chains and the link of the glucose monomers in the carbohydrates studied by Molinero and Goddard,[20] we determined the values of the parameters θ_0 (eq 3), φ_1°, φ_2°, and φ_3°, (eq 4) from the electron and X-ray diffraction data of the molecular and crystal structure of dextran reported by Guizard et al.;[28,29] these calculated values of θ_0, φ_1°, φ_2°, and φ_3°, are presented in Tables 1 and 2, respectively, of this work.

The nonbonded interaction between the coarse-grain beads of the dextran polymer chains, the interaction between the coarse-grain particles of the dextran and the water molecules,

TABLE 1: Values of the Angle-Bending Parameter θ_0 (eq 3)

angle type	θ_0 (deg)
161′	98.2
616′	85.2
461′	124.5
416′	120.8

TABLE 2: Values of the Torsion Angle Parameters φ_1°, φ_2°, and φ_3° (eq 4)

torsion type	φ_1° (deg)	φ_2° (deg)	φ_3° (deg)
616′1′	−159	−138	
461′4′	−146	−113	
461′6′	−110	−39	
416′1′	−164	−148	
6416′	−60		
1461′	−72		145
4161′	−128	−76	
4616′	−131	−83	
61′6′1"	−160		

and the interaction between the water molecules are considered to be described by the Morse potential.[20]

$$V(R_{ij}) = D_0\left[\left(\exp\left(-0.5\alpha\left(\frac{R_{ij}}{R_0} - 1\right)\right)\right)^2 - 2\left(\exp\left(-0.5\alpha\left(\frac{R_{ij}}{R_0} - 1\right)\right)\right)\right] \tag{5}$$

where R_{ij} is the distance between superatoms or water molecules *i* and *j*, R_0 is the distance of minimum energy D_0, and α is the measure of the curvature of the potential around R_0. The values of the parameters $D_{0,ij}$, $R_{0,ij}$, and α_{ij} for the cross interactions between unlike pairs are determined from the mixing rule as follows:[20]

$$D_{0,ij} = \sqrt{D_{0,i}D_{0,j}} \tag{6a}$$

$$R_{0,ij} = \sqrt{R_{0,i}R_{0,j}} \tag{6b}$$

$$\alpha_{ij} = \frac{1}{2}(\alpha_i + \alpha_j) \tag{6c}$$

The nonbonded Morse parameters for the coarse-grain particles (B1, B4, or B6) depend on whether the monomer is at the terminus or at an internal position of the chain.[20] Therefore, there are only six types of superatom parameters for the nonbonded interaction. From the crystal coordinates of dextran,[28,29] it is found that the three beads in one glucose monomer of dextran (α-D-(1 → 6)-linked glucan) occupy the same positions as the three beads in the glucose monomer of the α-D-(1 → 4)-linked glucans studied by Molinero and Goddard,[20] and this finding infers that the spatial distribution of the beads in the polymers composed of α-D-(1 → 4)-linked or α-D-(1 → 6)-linked glucans is similar. The values of the Morse parameters R_0, D_0, and α for the coarse-grain water were obtained from the data in Table 6 of ref 20.

In Figure 3, a schematic representation of the attachment of a dextran polymer chain on the surface of the base matrix, as well as the water molecules surrounding the beads of the polymer chain, are shown. As discussed above, in this work, 10 dextran polymer chains having either 25 or 40 monomers in each main polymer chain were randomly distributed on the 100 Å × 100 Å model surface, and periodic boundary conditions were applied along the lateral *x* and *y* directions. The locations of the side chains were chosen randomly on the main linear dextran chain such that a specific branching degree requirement

for the total number of dextran chains employed was reached; in the systems studied in this work, the degree of branching is 5%. One or two monomers were randomly chosen for the formation of a single side chain. In the coarse-grain model employed in this work, the side chains attach to the C4 position of the monomers in the main chain. Furthermore, the 30000 water molecules used in our simulation system formed a body of water along the z direction that is approximately equal to 130 Å. Because the upper part of the resultant dextran porous layer represents the region of most importance for affecting transport and adsorption of biomolecules for the reasons discussed earlier in this section, and because this upper region is located farthest from the surface on which the polymer chains are attached, the structureless surface model[16,17,30,31] is adopted and the effect of this surface model on the upper region of the dextran porous layer is considered to be small. The Morse potential was taken as the expression of the interaction between the model surface and dextran beads as well as water molecules in this system. To determine the relevant parameters of the model surface, it was considered that the surface is composed of saccharide beads and the arrangement of the beads on the most outer layer of the surface is random and the probability for the appearance of every type of coarse-grain particles is taken to be equal. Thus, the uniformly distributed surface beads could be modeled as aligned beads of only one type on the surface, and the interaction between the surface and the particles in the aqueous solution can be expressed by the interaction between the aqueous particles at a distance z from the surface with a single bead. The values of the parameters of the Morse potential for the model surface were determined to be as follows: the distance, R_0, of the minimum energy, D_0, is 5.31 Å, the value of the minimum energy, D_0, is 1.42 kcal/mol, and the parameter α that provides a measure of the curvature of the potential around R_0 is equal to 10.8.

The molecular dynamics simulations in this study were performed in the *NVT* ensemble. The equations of motion were integrated using the leapfrog algorithm,[26,27] and the time step employed was 5.0 fs. The system temperature was set at 298.15 K and controlled by applying the thermostat method of Brown and Clarke[32] to the water molecules and the dextran chains. The initial conformations of the dextran chains were based on repetition of the structure of dextran provided by Guizard et al.[28,29] An annealing procedure was used to expedite equilibration. The simulation system was first heated to and kept at 353.15 K for a period of time until the dextran chains and water molecules appeared to be uncorrelated with their initial conditions. The system was then cooled in a stepwise manner and reequilibrated at the set temperature ($T = 298.15$ K) for at least 1 ns, during which the water density and a number of potential energies were monitored as part of the equilibration criteria. It should be noted that, within 500 ps on the course of equilibration, the model dextran layers had reached stable structures that changed negligibly until the end of the simulation runs. Such stability can be attributed to the dextran chains' limited structural flexibility and complete immersion in liquid water, and alleviated the need of prolonged simulations for the structural characterization performed in this work.

As was discussed above, two systems employing 25 and 40 monomers per main polymer dextran chain, respectively, are studied in this work, and significant differences in the porous structures, as shown in the next section, in accord with experimental observations, can be obtained from these two model systems. The physical implications of the differences between the two systems were negligibly affected by the initial conditions of the distribution of the polymers on the surface of the base matrix.

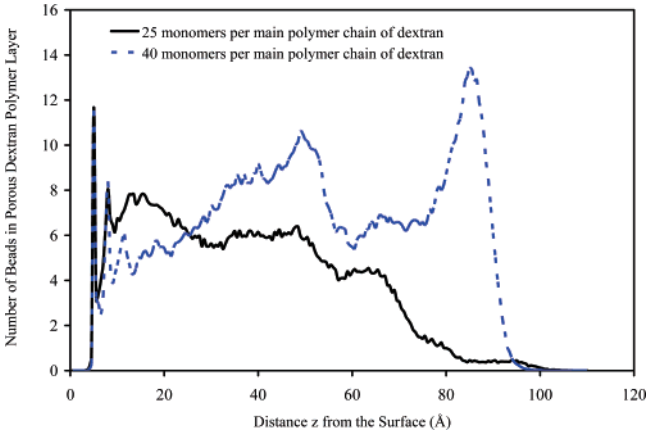

Figure 4. Number of beads in porous dextran polymer layer as a function of the distance from the surface of the base matrix.

Furthermore, it is worth mentioning here that the CPU time that would be required by an atomistic model to simulate the systems studied in this work, is estimated to be at least 500 times larger than the CPU time used by the modified M3B coarse-grain model employed in the simulations performed in this work.

3. Results and Discussion

In Figure 4, the number of beads from which the dextran polymer chains are comprised is presented as a function of the distance z from the surface on which the 10 dextran polymer chains are attached. The data in Figure 4 suggest that, when the dextran main polymer chain is composed of 25 monomers, then the distribution of the beads appears to be mainly unimodal, while the distribution of the beads seems to be represented by mainly a bimodal distribution when the dextran main polymer chain is composed of 40 monomers. It should be mentioned here that the peaks occurring in both systems at about $z \cong 5$ Å are due to the immobilized beads of the 10 dextran polymer chains that have been attached on the surface of the base matrix. The data in Figure 4 would suggest that, if the beads do not form locally large globules of beads having in each globule many beads in contact with each other, in the outer region of the dextran porous polymer layer there could be a few large pores and a rather small pore surface area when the porous layer is formed from 25 monomers per main polymer chain, while there could be a larger pore surface area at the outer region of the dextran porous polymer layer for the system where each main polymer chain has 40 monomers. This possible result could then imply that there could be a larger pore surface area in the outer region of the dextran porous polymer layer for the system whose main polymer chains have 40 monomers, and thus, a larger number of affinity groups/ligands could be attached on the pore surface area during the process of Stage II, considering, of course, that the size of the pore openings is large enough to allow the penetration of the affinity groups/ligands into the pore space of the outer region of the polymer layer so that they could be attached on most of the available pore surface area. This implied result from the data in Figure 4 appears to be consistent with experimental observations.[7,19] It is worth mentioning at this point that the degree of flexibility of the outer part of the dextran polymer, whose main chain has 40 monomers, is larger than that of the dextran polymer whose main chain has 25 monomers.

Two of the important variables, whose determination is used in practice as members of the set[12,13,33−39] of variables that characterize the structure of a porous medium, are the total pore volume and the size distribution of the pore volume. In the material that follows in this paragraph, the procedure developed in this work and used to determine these two parameters for the structures of the porous polymer layers constructed by MD simulations, is presented. The dimensions of the volume element of the dextran porous layers studied in this work, that includes both the pore space and the space occupied by the beads of the polymer chains, are 100 Å along each of the lateral *x* and *y* directions, while the length along the *z* direction starts at $z = 0$ and ends at the highest value of *z*, which is located on the uppermost surface of the bead of the dextran polymer chains that is farthest located from the surface on which the polymer chains are attached. In each system studied in this work, the coordinates along the *x*, *y*, and *z* directions of each bead of the dextran polymer chains are known, and therefore, the coordinates of the three-dimensional (3D) structure of the porous polymer layer of each system is known; thus, because of this, the total pore volume and distribution of the topology of the pore space (the space unoccupied by the beads of the dextran polymer chains) in the volume element of each system can be determined. To determine the size distribution of the pore volume, the volume element of each system studied here was divided into a lattice of cubes, where the dimension along each of the *x*, *y*, and *z* directions of each cube is 3.3 Å; this size was selected because it is approximately equal to the size of a water molecule. The volume of each cube was then divided into a lattice of cubic cells, where the dimension along each of the *x*, *y*, and *z* directions of each cubic cell is 0.3 Å. Thus, this approach involves a two-level lattice representation with the space associated with the volume element of each system studied in this work and was found to provide computational efficiency and satisfactory accuracy in determining the size distribution of the pore volume. Spherical probes of varying diameters are employed in the cubes of the two-level lattice, and by knowing the position of the beads of the dextran polymer chains in the *x*, *y*, *z* space, the volume of the beads is then excluded and the volume of the pore space that corresponds to the diameter of a spherical probe is evaluated.

By implementing the above-mentioned computational procedure and considering all the pore volumes with size greater than or equal to the diameter of a water molecule (∼3.2 Å), it is found that the values of the porosity of the systems having 25 and 40 monomers per main polymer chain of dextran are 68.92% and 64.77%, respectively. The pore volumes associated with different sizes of pore openings (size distribution of the pore volume of porous polymer layer) for the systems having 25 and 40 monomers per main polymer chain are shown in the histograms presented in Figures 5 and 6, respectively. The data in Table 3 clearly indicate that the porous polymer layers formed by the beads have a large number of small-size pores and a small number of large-size pores, while the results in Figures 5 and 6 show that the pore openings represented by the smaller and larger sizes together account for an amount of pore volume that is more than 50% of the total pore volume. Furthermore, the data in Table 3 show that the system having 40 monomers per main polymer chain of dextran has a considerably larger number of pore openings in the range of pore sizes from 10 to 32 Å, and this result, together with the pore volume data in Figures 5 and 6, and the fact that the results in Figure 4 suggest, as discussed above, that there could be many more pores in the outer region of the porous polymer layer composed of 40

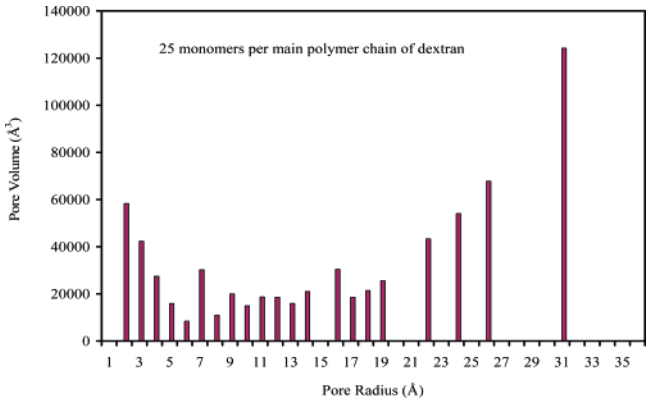

Figure 5. Histogram representing the pore volume corresponding to different ranges of pore radii in the porous polymer layer having 25 monomers per main polymer chain of dextran.

Figure 6. Histogram representing the pore volume corresponding to different ranges of pore radii in the porous polymer layer having 40 monomers per main polymer chain of dextran.

monomers per main polymer chain than in the system having 25 monomers per main polymer chain, imply that there will be a larger number of proper size pore openings and a larger pore surface area available for the corresponding transport and subsequent attachment of affinity groups/ligands in the porous polymer layer composed of 40 monomers per main polymer chain of dextran during the operation of Stage II that concerns itself with the introduction and immobilization on the pore surfaces of the affinity groups/ligands. Thus, the results in Table 3 and Figures 4−6 could suggest that, at the end of the sequence of Stages I and II, the porous polymer layer composed of 40 monomers per main polymer chain of dextran could have (i) a larger number of immobilized affinity groups/ligands (adsorption sites) on its pore surfaces, and (ii) a larger number of proper-sized pores located at the outer region of its porous structure to facilitate the operation of Stage III that involves the transport and adsorption of the biomolecule of interest than the porous polymer layer composed of 25 monomers per main polymer chain. Of course, it should be mentioned here that the size of the biomolecule of interest should be smaller than the size of the pores, resulting in the outer region of the porous polymer layer after the immobilization of the affinity groups/ligands. It is important to note here that (a) the size distribution of the pores and (b) the number of pore openings along the lateral planes at different positions *z* from the surface of the base matrix that provide connections to pathways that effectively facilitate the transport and adsorption of a biomolecule of interest whose size is known depend on the type and length of the polymeric extender, the number of attachment points to the base matrix per molecule of extender, the degree of side branching of the

TABLE 3: Number of Pore Openings Corresponding to Different Ranges in the Values of the Radii of the Pore Openings

range of values of radii of pore openings (Å)	number of pore openings for system with 25 monomers per main polymer chain of dextran	number of pore openings for system with 40 monomers per main polymer chain of dextran
1.6−2	2514	2388
2−3	935	913
3−4	182	159
4−5	31	45
5−6	19	36
6−7	22	29
7−8	8	11
8−9	7	6
9−10	7	8
10−11	2	2
11−12	3	6
12−13	2	3
13−14	2	3
14−15	0	1
15−16	2	2
16−17	1	0
17−18	2	3
18−19	0	1
19−20	0	0
20−21	0	0
21−22	1	0
22−23	0	2
23−24	1	1
24−25	0	0
25−26	1	0
26−27	0	0
27−28	0	0
28−29	0	0
29−30	0	0
30−31	0	0
31−32	1	0

extender, the number of extender molecules immobilized per unit surface area of base matrix, and the size, number, and location of the affinity groups/ligands on the branched extender molecules. A major goal of this work is to present a methodology based on MD modeling and simulation studies that, after knowing the type and size of an affinity group/ligand that will be used as an adsorption site and the size of the biomolecule that will be adsorbed onto the affinity group/ligand, could be used to construct different porous dextran layers by varying the length of the polymer chain of dextran, the number of attachment points to the base matrix, the degree of side branching, and the number of main polymer chains immobilized per unit surface area of base matrix; the analysis, characterization, and evaluation of different porous dextran layers generated would enable a researcher to select one or more promising porous structures in order to proceed in performing Stages II and III, whose functions have been discussed in the Introduction section. The methodology (based on MD modeling and simulation studies) developed and presented in this work has produced two different porous polymer layers, whose structures have been characterized up to this point by the results in Table 3 and Figures 4−6, and the importance of the implications of these results was discussed above. It is also interesting and physically consistent that the implications of the results in Table 3 and Figures 4−6 are also confirmed by the results in Figures 7 and 8, where the spatial distribution in three dimensions of the dextran beads forming the upper part of the porous polymer layers having 25 and 40 monomers per main polymer chain of dextran, respectively, is presented. The results in Figure 7 clearly show that the upper part of the porous layer formed from dextran chains having 25 monomers per main polymer chain, has a small number of beads whose contacts with each other are so few that pore openings of only very large radii are formed, and these pores in the upper

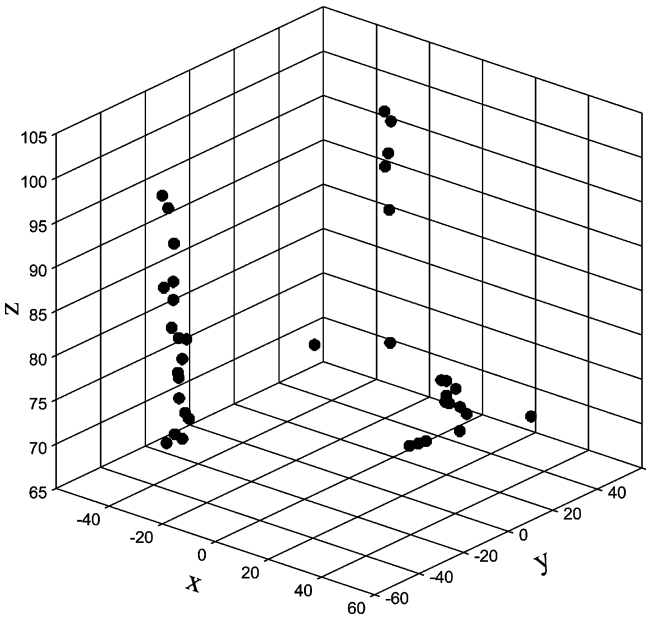

Figure 7. Spatial distribution in three dimensions of the beads forming the upper region of the porous dextran layer having 25 monomers per main polymer chain of dextran.

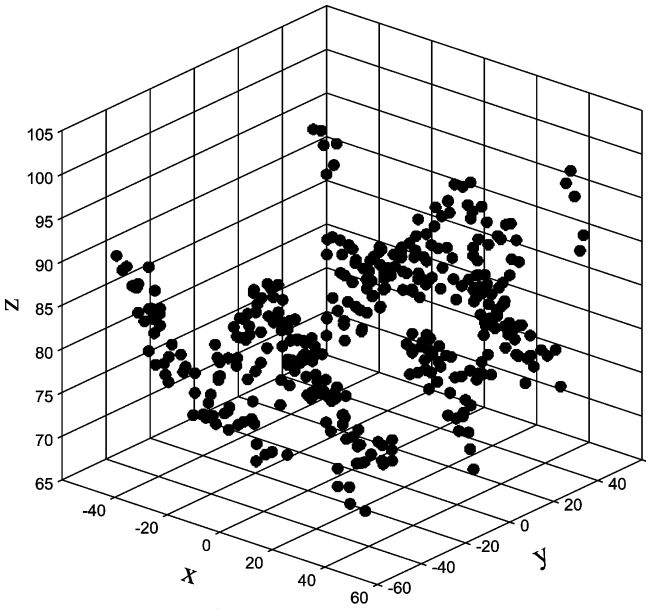

Figure 8. Spatial distribution in three dimensions of the beads forming the upper region of the porous dextran layer having 40 monomers per main polymer chain of dextran.

region of the polymer structure have a very small pore surface area for the subsequent attachment of affinity groups/ligands. The results in Figure 8 show that the upper part of the porous layer of the system constructed from dextran chains having 40 monomers per main polymer chain has a larger number of beads whose contacts with each other are many more than those of the system in Figure 7, and thus, the upper porous structure of the system in Figure 8 has many more pores of intermediate and large radii, and these pores are significantly more useful operationally than those of the system in Figure 7 because they provide a significantly larger pore surface area for the attachment of affinity groups/ligands. While the results in Figures 7 and 8 confirm the physical implications of the data in Table 3 and Figures 4−6 in a physically consistent manner, it is thought that the data in Figures 7 and 8 additionally provide a lucid

graphical representation about the relative magnitudes of the pore surface areas associated with the upper region of the porous polymer layers of the two different systems represented in Figures 7 and 8.

Another important parameter used in the characterization of porous media is the pore connectivity parameter employed in pore network[34,36−56] models and represents, for any given lattice that is used to construct the pore network, the product of the percolation and coordination numbers of the lattice. Therefore, once a set of pores are mapped onto the lattice and the pore network is constructed, the pore connectivity represents the average number of pores that are assigned to one node in the lattice; it should be noted that, depending on the type of pore mapping procedure that is employed (semirandom mapping or totally random mapping), the distribution of the pore connectivity over the lattice can be narrow (semirandom mapping) or very wide (totally random mapping), and the connectivity distributions for any type of pore mapping procedure do not converge until the pore connectivity approaches the coordination number of the lattice (fully connected lattice). The discrete network of interconnected pores in the network model can be used to study the effect and relative importance of percolation in porous media for different processes, and when the equations that describe a pore characterization process (e.g., mercury intrusion, size exclusion chromatography) are applied to each pore in the network, after a geometry (e.g., cylindrical) has been assigned to the pores, and used to simulate the experimental data obtained from a characterization process on a physically real porous medium (e.g., porous adsorbent particles, porous catalysts), a value for the pore connectivity can be obtained to characterize the porous medium in addition to the distribution of pore sizes (size distribution of the pore volume). However, the pore connectivity obtained from pore network modeling is a model parameter, and thus, the pore connectivity does not represent the true connectivity of the real porous medium, but only the connectivity of the lattice employed in the network model that will best represent the experimental data. Consequently, if one employs a lattice in their network model that has a sufficiently high coordination number, there will exist a critical pore connectivity value, where for all values of the pore connectivity larger than this critical value, the pore network behaves as an infinitely connected bundle of pores arranged in parallel (parallel pore model). In this case, one cannot determine a unique value of the pore connectivity for a material above this critical value, and this critical value might not be independent of the experimental process used to characterize the porous media. The dependence of the meaning of the pore connectivity parameter on the lattice employed in the network model, and the inability of the network model, as discussed above, to determine a unique and finite pore connectivity for real porous materials, whose properties are such that the results from pore characterization with a network model approach the results obtained from parallel pore models, represent a drawback of pore network theory. Furthermore, the isolated and dead-end pores that appear in the model porous medium when the percolation number of the lattice approaches the percolation threshold also pose a problem when trying to match the porosities of the network to the porosity of the real porous medium. Of course, one can consider the pore volume of the isolated and dead-end pores in the model to be part of the inaccessible volume in a percolation pathway in the real porous medium, but by removing (or neglecting) these pores in the calculation of transport coefficients in the model porous medium, one still would have lost the match between the porosity of the model porous medium and the porosity of the real porous medium.

Despite these limitations, the pore size distributions, both on a number basis (number of pores of a certain size) and on a volume basis (size distribution of pore volume), and the pore connectivity determined from employing pore network models to the experimental data obtained from pore characterization experiments where the real porous medium is used, serve as an input to a network model (discrete microscopic model) that is employed to estimate the values of the intraparticle effective pore diffusion coefficient and velocity for a given solute of interest in packed beds and monoliths employed in separation and chemical and biochemical reaction engineering systems, and whose behavior is described by macroscopic continuum models that use in their intraparticle diffusion and convection mechanisms the values of the effective pore diffusion coefficient and velocity estimated from the pore network model. While the agreement between the experimental data and the theoretical results obtained from the macroscopic continuum models may not be perfect (which could be due to a number of other parameters employed in the macroscopic continuum models and whose values may not be well-known, such as the axial dispersion coefficient or the parameters associated with adsorption and/or chemical and biochemical reaction kinetics), the transport parameters estimated from the network model almost always provide the correct trend in the data and, more importantly, allow one to identify the main feature of the structure of the porous medium that bottlenecks the performance of the packed bed or monolith. For this reason, pore network models as a pore characterization and predictive modeling tool play currently a very useful and practical (the computational times involved in pore network modeling calculations are not significantly long) role in the multiscale modeling approach used in practice and discussed above, despite the discrepancy between the pore connectivity of the pore network model and the pore connectivity of the real porous medium. In the following paragraph, a conceptual definition of pore connectivity that could be operationally useful for characterizing real porous media is developed by utilizing the three-dimensional structure information that we have determined (as discussed above) for the two different porous polymer layers we have constructed by using the MD modeling and simulations methodology presented in this work.

As we discussed above, the spatial distribution in three dimensions of all the beads of the dextran polymers is known for both porous polymer layers formed by 25 and 40 monomers per main polymer chain, respectively, and the size, number, and location of the pore openings in the three-dimensional space is known. In Figures 9 and 10, the number of pore openings as a function of the distance z from the surface of the base matrix and for different ranges of the radii of pore openings are presented for the porous polymer layers having 25 and 40 monomers per main polymer chain, respectively; the pore openings with radii in the range 1.6−5.0 Å are not presented in Figures 9 and 10 because pores of such sizes are considered to be operationally not useful for utilizing them to immobilize affinity groups/ligands because their small size could be comparable to or smaller than the size of the affinity groups/ligands. It is worth mentioning here that the increment of 5 Å that defines the largest difference in the magnitudes of the pore radii considered in each range of values of pore radii indicated in Figures 9 and 10 (as well as in Figures 11 and 12 discussed later on) was selected on the basis of the conventional

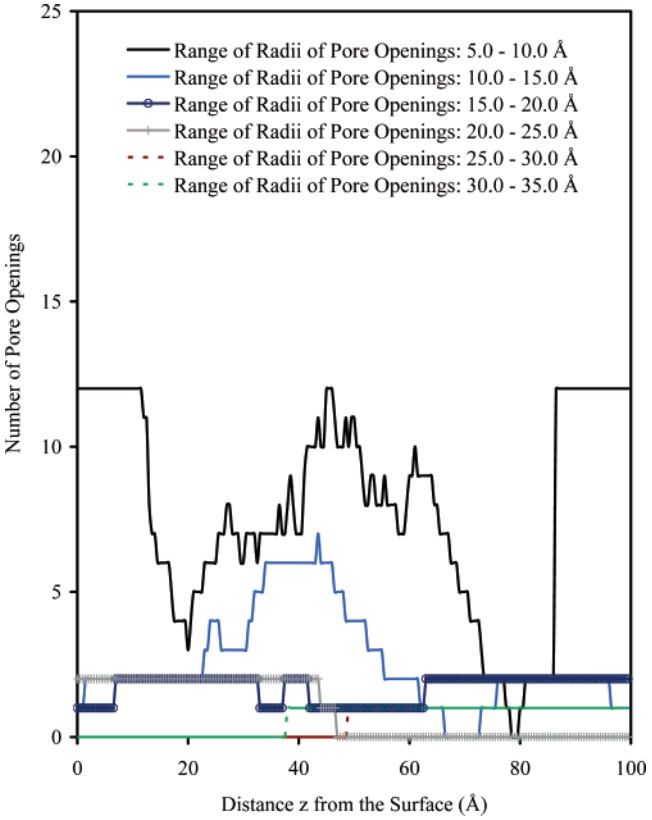

Figure 9. Number of pore openings as a function of distance z from the surface for different ranges of pore radii when the porous polymer layer has 25 monomers per main polymer chain of dextran.

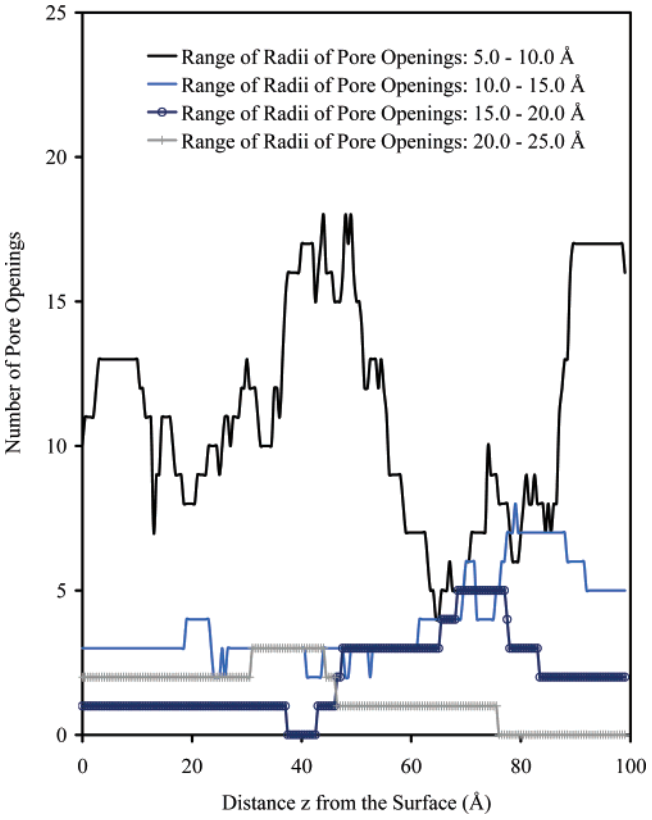

Figure 10. Number of pore openings as a function of distance z from the surface for different ranges of pore radii when the porous polymer layer has 40 monomers per main polymer chain of dextran.

consideration where, in histograms representing pore volumes for different pore sizes, the increment employed between pore

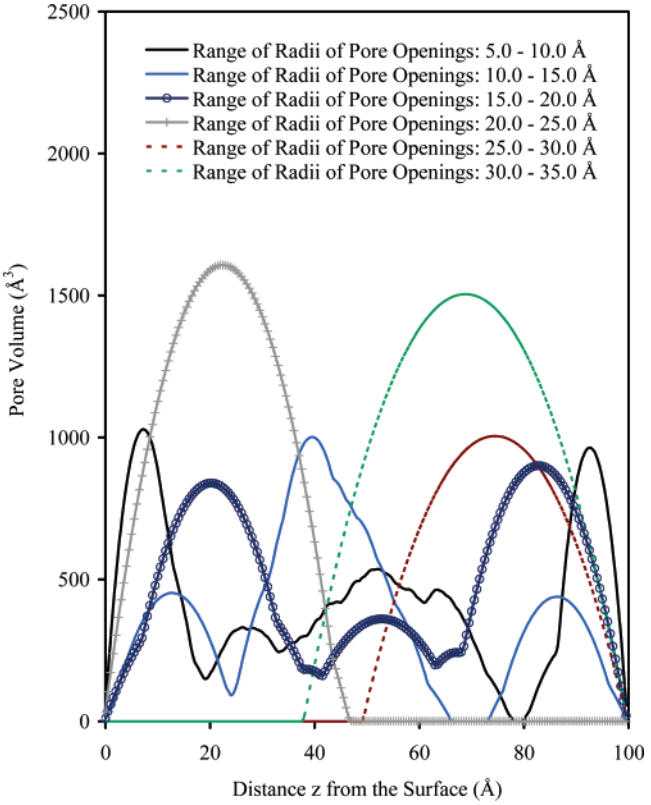

Figure 11. Pore volume determined by considering the pore volumes of the pore openings over a length interval, Δz, of 0.5 Å along the z direction for different ranges of pore radii when the porous polymer layer has 25 monomers per main polymer chain of dextran.

sizes is often taken to be equal to 5 Å so that the information on the histogram is not cluttered; but, of course, a different magnitude for this increment could have been selected. The results in Figure 9 show that (i) the number of pore openings along the z direction has discontinuities (a discontinuity denotes that the number of pore openings is equal to zero for a given range of pore radii) for all ranges of pore radii, (ii) the frequency and length along the z direction of these discontinuities are not small, and (iii) there are a few positions along the z direction where ranges of different pore radii have the same number of pore openings on the same lateral plane. Furthermore, the number of pores involved from each range of different pore radii is rather small. On the contrary, the results in Figure 10 show that (a) there is only one discontinuity along the z direction and it is associated with the range of pore radii being between 15.0 and 20.0 Å, while it is worth noting here that the location at the uppermost surface of the porous polymer layer, where the pore openings having radii 20.0−25.0 Å originate, is at z = 75.5 Å, and therefore, this position of z does not represent a point of discontinuity in Figure 10, (b) the length along the z direction of the single discontinuity is small, and there are many pore openings of different sizes on the lateral planes located above the position z = 43.5 Å, where the discontinuity occurs, (c) the average total number of pore openings on a given lateral plane in Figure 10 is significantly larger than that in Figure 9 and (d) the length along the z direction (starting from the largest value of z in the uppermost surface of the porous polymer layer and proceeding toward the surface of the base matrix) over which there are large numbers of pores of different pore radii is significantly larger than that of the system in Figure 9, and this could imply that the total number of direct and alternative conducting pathways for transport in the system of Figure 10 could be larger than that of the system in Figure 9. Furthermore,

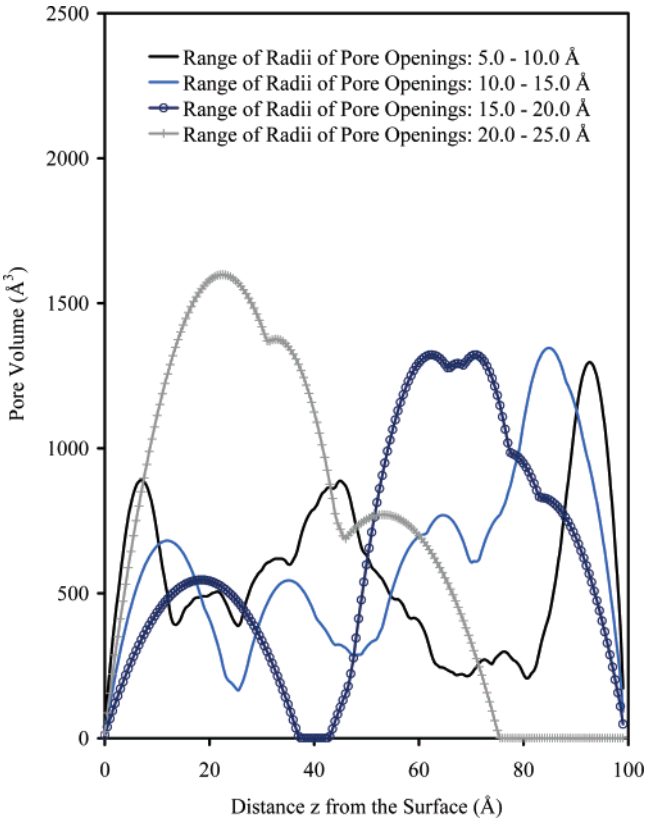

Figure 12. Pore volume determined by considering the pore volumes of the pore openings over a length interval, Δz, of 0.5 Å along the z direction for different ranges of pore radii when the porous polymer layer has 40 monomers per main polymer chain of dextran.

the total number of pore openings for the system in Figure 10 in the region of z between 43.5 and 100 Å, which is considered to represent the region that would be most useful for the transport and subsequent attachment of the affinity groups/ligands, is significantly larger than that of the system in Figure 9. The discussion for the results in Figures 9 and 10 clearly indicates that the porous polymer layer having 40 monomers per main polymer chain provides a significantly larger number of conducting pathways for the transport of a solute from the outer surface of the porous layer to most of the interior of the porous medium than the porous polymer layer having 25 monomers per main polymer chain. It is also worth mentioning here that the results in Figures 9 and 10 clearly show the spatial tortuous nature along the z direction of the conducting pathways that facilitate transport along the direction of net transport (along the z direction) in the porous dextran polymer layer. Furthermore, the results in Figures 9 and 10 and the analysis and discussion of the results in these figures suggest that a useful definition of pore connectivity for a real porous medium could be as follows: the pore connectivity represents a measure of the number of conducting pathways that facilitate transport along the direction of net transport in a porous medium, and the magnitude of this number of conducting pathways is related to the average total number of pore openings of different pore radii located on the lateral planes, which are normal to the direction of net transport and to the size of length along the direction of net transport originating from the outermost surface of the porous medium and ending at the point in the direction of net transport where a discontinuity in a significant number of pore openings of different conducting ranges of pore radii occurs. It should be noted here that this definition of the pore connectivity of a real porous medium is significantly different than the artificial physical meaning associated with this parameter in pore network models, which are supposed to represent model porous media that are used to simulate the transport behavior of real porous media.

In Figures 11 and 12, the pore volume as a function of the distance z from the surface of the base matrix and for different ranges of the radii of pore openings are presented for the porous polymer layers having 25 and 40 monomers per main polymer chain, respectively; the pore openings with radii in the range 1.6−5.0 Å are not presented in Figures 11 and 12 for the same reason as discussed above for Figures 9 and 10. It should be mentioned here that the volumes in Figures 11 and 12 were determined by considering the pore volumes of the pore openings over a length interval, Δz, of 0.5 Å along the z direction. In Figures 11 and 12, the curves that are smooth and do not have even a single shoulder represent pore volumes associated with a single void space in the porous medium, which has the range of pore radii associated with the smooth curves. Shoulders on a given curve denote that there are more than one void space (multiple void spaces) in the porous medium having the range of pore radii for their pore openings associated with the given curve. Thus, the larger the number of shoulders on a given curve, the larger is the number of void spaces in the porous polymer layer having the range of pore radii for their pore openings associated with the given curve. For a given curve, the starting point of the curve in the z direction is taken to be the largest value of z at which the curve begins, while the ending point of the curve is taken to be the smallest value of z at which the curve ends. A discontinuity in Figures 11 and 12 for a given curve is defined as a position in the z direction in the range $0 < z < 100$, where the value of the pore volume becomes equal to zero at the ending point of the given curve. By comparing the results in Figures 11 and 12, it is observed that the system in Figure 12 having 40 monomers per main polymer chain (i) has many more void spaces in its porous structure over a significantly larger length along the net transport direction z for a given range of pore radii than the system in Figure 11, and this significantly larger number of void spaces is especially dominant in the outer region of the porous layer between $z =$ 43.5 Å and $z = 100$ Å, which is considered to represent the region that would be most useful for the transport and subsequent attachment of the affinity groups/ligands, and (ii) has only one discontinuity, while the system in Figure 11 has many more discontinuities. Again, as was discussed for Figure 10, it is worth noting here that, in Figure 12, the location at the uppermost surface of the porous polymer layer where the pore openings having radii 20.0−25.0 Å originate, is at $z = 75.5$ Å. Two additional important variables of interest in the characterization of porous media are those associated with the pore surface area and its distribution along the net direction of transport. The results in Figures 11 and 12 can be considered to provide a relative measure with respect to the pore surface areas and their corresponding distributions along the net direction of transport, z, for the two different porous structures. The results in Figures 11 and 12 indicate that the porous layer having 40 monomers per main polymer chain has a relatively larger and better distributed along the z direction pore surface area than the porous layer having 25 monomers per main polymer chain, and this positive result for the porous structure of the system in Figure 12 is more profound in the outer region of the porous layer (43.5 Å $\leq z \leq$ 100 Å), which is considered to represent the region that would be most useful for the transport and subsequent adsorption of the affinity groups/ligands. The more desirable practical implications with respect

to structural properties exhibited by the comparison of the results in Figures 9−12 for the system having 40 monomers per main polymer chain are mainly due to the higher flexibility of the polymer chains of this system, especially in the upper region of the porous structure.

High-resolution noninvasive methods based on NMR and MRI[50,54] as well as high-resolution optical[57,58] microscopy methods are being developed to provide the data of the three-dimensional representation of the structure of real porous media. Such three-dimensional data could be used to determine and represent results for the real porous media of the form presented in Figures 9−12. Furthermore, the three-dimensional data of the real porous structures could make it possible, in principle, to simulate the transport and adsorption or transport and chemical/biochemical reaction of a solute(s) in the real porous media by solving the continuity equation(s) of the solute(s), as well as the electrostatic potential equation[10−13,15−17,59] in the geometry of the void spaces of the real porous media (even if mathematical techniques such as conformal mapping may have to be employed because of the geometric shape of the pores of the real porous media) without having to resort to the use of pore network models whose physical limitations were discussed above. It is thought that, on the basis of the current relative successes of different high-resolution noninvasive methods to provide accurate[57,58] three-dimensional information on the structure of real porous media, whose pores have radii larger than or equal to 500 Å, high-resolution optical[57,58] microscopy methods could provide in the rather near future the means to determine by three-dimensional optical microscopy the structure of real porous media having pore radii smaller than 500 Å.

4. Conclusions and Remarks

The M3B model was modified and used in MD simulation studies to construct porous dextran layers on the surface of a base matrix where the dextran polymer chains and the surface of the base matrix are covered by water. The MD modeling and simulations presented in this work provide a methodology that could be used, considering that the type and size of the affinity group/ligand that will be used as an adsorption site and the size of the biomolecule that will be adsorbed onto the affinity group/ligand are known, to construct different porous dextran layers by varying the length of the polymer chain of dextran, the number of attachment points to the base matrix, the degree of side branching, and the number of main polymer chains immobilized per unit surface area of base matrix. The methodology presented here was used to construct two different porous dextran layers having 25 and 40 monomers per main polymer chain.

Furthermore, the types of three-dimensional structural information that could be used to characterize the porous structures generated by the MD modeling and simulation studies were presented, and it was found that the porous layer formed by the dextran polymer chains having 40 monomers could provide a more suitable porous medium for the transport in the pore spaces and subsequent attachment of the affinity groups/ligands on the surface of the pores than the porous layer formed by the dextran polymer chains having 25 monomers per main polymer chain. The more desirable practical implications with respect to structural properties exhibited by the system having 40 monomers per main polymer chain are mainly due to the higher flexibility of the polymer chains of this system, especially in the upper region of the porous structure. Also, the analysis and discussion with regard to the characterization of the porous polymer layers have suggested a useful definition for the physical meaning and implications of the pore connectivity of a real porous medium with respect to the number of conducting pathways along the direction of net transport in the real porous medium, and this definition is significantly different than the artificial physical meaning associated with the pore connectivity parameter employed in pore network models, which are used to simulate the transport behavior in real porous media.

Finally, it was discussed how three-dimensional information about the structure of a real porous medium obtained from noninvasive techniques, such as high-resolution optical three-dimensional microscopy methods, could be used together with the continuity expression of a solute and the electrostatic potential equation to simulate, for instance, transport and adsorption in ion-exchange porous adsorbent particles without having to resort using pore network models whose physical limitations were also discussed in this work.

References and Notes

(1) Yamamoto, S.; Nakanishi, K.; Matsuno, R. *Ion-Exchange Chromatography of Proteins*; Marcel Dekker: New York, 1988.
(2) Harrison, R. G.; Todd, P.; Rudge, S. R.; Petrides, D. P. *Bioseparations Science and Engineering*; Oxford University Press: New York, 2003.
(3) Poole, C. F. *The Essence of Chromatography*; Elesevier: Amsterdam, The Netherlands, 2003.
(4) Boschetti, E. *J. Chromatogr., A* **1994**, 658, 207.
(5) Levison, P. R.; Mumford, C.; Streater, M.; Brandt-Nielsen, A.; Pathirana, N. D.; Badger, S. E. *J. Chromatogr., A* **1997**, *760*, 151.
(6) Gibert, S.; Bakalava, N.; Santarelli, X. *J. Chromatogr., B* **2000**, *737*, 143.
(7) Berg, H.; Hansson, H.; Kagedal, L. Adsorption/Separation Method and a Medium for Adsorption/Separation, U.S. Patent, US 6,428,707 B1, August 6, 2002.
(8) Johansson, B.-L.; Belew, M.; Eriksson, S.; Glad, G.; Lind, O.; Maloisel, J.-L.; Norrman, N. *J. Chromatogr., A* **2003**, *1016*, 21.
(9) Johansson, B.-L.; Belew, M.; Eriksson, S.; Glad, G.; Lind, O.; Maloisel, J.-L.; Norrman, N. *J. Chromatogr., A* **2003**, *1016*, 35.
(10) Liapis, A. I.; Grimes, B. A.; Lacki, K.; Neretnieks, I. *J. Chromatogr., A* **2001**, *921*, 135.
(11) Grimes, B. A.; Liapis, A. I. *J. Colloid Interface Sci.* **2002**, *248*, 504.
(12) Grimes, B. A.; Lüdtke, S.; Unger, K. K.; Liapis, A. I. *J. Chromatogr., A* **2002**, *979*, 447.
(13) Grimes, B. A.; Liapis, A. I. *J. Sep. Sci.* **2002**, *25*, 1202.
(14) Sikavitsas, V.; Nitsche, J. M.; Mountziaris, T. J. *Biotechnol. Prog.* **2002**, *18*, 885.
(15) Zhang, X.; Grimes, B. A.; Wang, J.-C.; Lacki, K. M.; Liapis, A. I. *J. Colloid Interface Sci.* **2004**, *273*, 22.
(16) Zhang, X.; Wang, J.-C.; Lacki, K. M.; Liapis, A. I. *J. Colloid Interface Sci.* **2004**, *277*, 483.
(17) Zhang, X.; Wang, J.-C.; Lacki, K. M.; Liapis, A. I. *J. Colloid Interface Sci.* **2005**, *290*, 373.
(18) Liapis, A. I. *Ind. Eng. Chem. Res.* **2005**, *44*, 5380.
(19) Lacki, K. M. GE Healthcare, Amersham Biosciences, Uppsala, Sweden. Personal communication, 2003.
(20) Molinero, V.; Goddard, W. A. *J. Phys. Chem. B* **2004**, *108*, 1414.
(21) Shelley, J. C.; Shelley, M. Y.; Reeder, R. C.; Bandyopadhyay, S.; Klein, M. L. *J. Phys. Chem. B* **2001**, *105*, 4464.
(22) Marrink, S. J.; Vries, A. H.; Mark, A. E. *J. Phys. Chem. B* **2004**, *108*, 750.
(23) Dickey, A. N.; Faller, R. *Polymer Physics* **2005**, *43*, 1025.
(24) Kreer, T.; Metzger, S.; Müller, M.; Binder, K. *J. Chem. Phys.* **2004**, *120*, 4012.
(25) Yaneva, J.; Milchev, A.; Binder, K. *J. Chem. Phys.* **2004**, *121*, 12632.
(26) Rapaport, D. C. *The Art of Molecular Dynamics Simulation*; Cambridge University Press: New York, 1995.
(27) Allen, M. P.; Tildesley, D. J. *Computer Simulation of Liquids*; Clarendon Press: Oxford, U.K. 1987.
(28) Guizard, C.; Chanzy, H.; Sarko, A. *Macromolecules* **1984**, *17*, 100.
(29) Guizard, C.; Chanzy, H.; Sarko, A. *J. Mol. Biol.* **1985**, *183*, 397.
(30) Steele, W. A. *Surf. Sci.* **1973**, *36*, 317.
(31) Toxvaerd, S. *J. Chem. Phys.* **1981**, *74*, 1998.
(32) Brown, D.; Clarke, J. H. R. *Mol. Phys.* **1984**, *51*, 1243.
(33) Dullien, F. A. L. *Porous Media: Fluid Transport and Pore Structure*, 2nd ed.; Academic Press: New York, 1992.
(34) Stauffer, D.; Aharony, A. *Introduction to Percolation Theory*, 2nd ed.; Taylor and Francis: London, 1992.

(35) Frey, D. D.; Schweinheim, E.; Horvath, Cs. *Biotechnol. Prog.* **1993**, *9*, 273.
(36) Liapis, A. I. *Math. Modelling and Sci. Computing* **1993**, *1*, 397.
(37) Meyers, J. J.; Liapis, A. I. *J. Chromatogr., A* **1998**, *827*, 197.
(38) Meyers, J. J.; Liapis, A. I. *J. Chromatogr., A* **1999**, *852*, 3.
(39) Meyers, J. J.; Crosser, O. K.; Liapis, A. I. *J. Biochem. Biophys. Methods* **2001**, *49*, 123.
(40) Koplik, J.; Lasseter, T. J. *Chem. Eng. Commun.* **1984**, *26*, 285.
(41) Koplik, J.; Redner, S.; Wilkinson, D. *Phys. Rev. A* **1988**, *37*, 2619.
(42) Rege, S. D.; Fogler, H. S. *AIChE J.* **1988**, *34*, 1761.
(43) Sahimi, M.; Jue, V. L. *Phys. Rev. Lett.* **1989**, *62*, 629.
(44) Petropoulos, J. H.; Liapis, A. I.; Kolliopoulos, N. P.; Petrou, J. K.; Kanellopoulos, N. K. *Bioseparation* **1990**, *1*, 69.
(45) Imdakm, A. O.; Sahimi, M. *Chem. Eng. Sci.* **1991**, *46*, 1977.
(46) Portsmouth, R. L.; Gladden, L. F. *Chem. Eng. Sci.* **1991**, *46*, 3023.
(47) Petropoulos, J. H.; Petrou, J. K.; Liapis, A. I. *Ind. Eng. Chem. Res.* **1991**, 30, 1281.
(48) Hollewand, M. P.; Gladden, L. F. *Chem. Eng. Sci.* **1992**, *47*, 1761.
(49) Meyers, J. J.; Nahar, S.; Ludlow, D. K.; Liapis, A. I. *J. Chromatogr., A* **2001**, *907*, 57.
(50) Latour, L. L.; Kleinberg, R. L.; Mitra, P. P.; Sotak, C. H. *J. Magn. Reson.* **1995**, *112*, 83.
(51) Bryntesson, L. M. *J. Chromatogr., A* **2002**, *945*, 103.
(52) Düren, T.; Jakobtorweihen, S.; Keil, F. J.; Seaton, N. A. *Phys. Chem. Chem. Phys.* **2003**, *5*, 369.
(53) Ghassemzadeh, J.; Sahimi, M. *Chem. Eng. Sci.* **2004**, *59*, 2265.
(54) Lori, N. F.; Conturo, T. E.; Bihan, D. L. *J. Magn. Reson.* **2003**, *165*, 185.
(55) Zalc, J. M.; Reyes, S. C.; Iglesia, E. *Chem. Eng. Sci.* **2004**, *59*, 2947.
(56) Armatas, G. S.; Pomonis, P. J. *Chem. Eng. Sci.* **2004**, *59*, 5735.
(57) Klar, T. A.; Jacobs, S.; Dyba, M.; Egner, A.; Hell, S. W. *Proc. Natl. Acad. Sci. U.S.A.* **2000**, *97*, 8206.
(58) Egner, A.; Jacobs, S.; Hell, S. W. *Proc. Natl. Acad. Sci. U.S.A.* **2002**, *99*, 3370.
(59) Liapis, A. I.; Grimes, B. A. *J. Sep. Sci.* **2005**, *28*, 1909.